

Chair of Optoelectronics
Institute for Computer Engineering
Ruprecht-Karls-University Heidelberg

Annual Report

2008 - 2010

Contents

Foreword	2
Research Projects	3
Publications	18
Imprint	22

Foreword



Dear reader,

This annual report covers the period from 2008 to 2010. It also marks the transition from the university of Mannheim to the university of Heidelberg, which of course was associated with plenty of organizational work. Officially the Mannheim-label was dropped with the end of 2007 and since January of 2008, the chair is officially a member of the Heidelberg faculty of Physics and Astronomy and a member of the institute of computer engineering (ZITI)".

This new institute was established as a central institution of the University of Heidelberg. Its six member chairs are assigned equally to the Department of Physics and Astronomy and the Department of Mathematics and Computer Science and have successfully integrated themselves into the research landscape of Heidelberg. At the same time, the institute was involved in implementing the Bologna process, which implied termination of the existing Diploma-program, an integration into an existing Bachelor program and the formation of a new Master program. This newly established Master of Computer Engineering has started this winter term 2011/12.

With this transition from Heidelberg to Mannheim, the research work of the chair also has shifted slightly toward more fundamental aspects of modern optics. Some contributions deal with the computational aspects of light in optical components (3, 4, 5, 7), some with mathematical aspects of controlling light (1, 2, 6) and several contributions also deal with applications in optical interconnects (9, 10, 13) and parallel optical microscopy (8, 11, 12). It is assumed, that from now on, the annual report will continue on a yearly basis.

Karl-Heinz Brenner
Head of the chair

Research Projects

1. Full control of light intensity by beam shaping	
<i>K.-H. Brenner</i>	5
2. Parallel image scanning with binary phase gratings	
<i>R. Buschlinger, K.-H. Brenner</i>	6
3. Vector wave propagation method (VWPM)	
An extension to the wave propagation method	
<i>M. Fertig, K.-H. Brenner</i>	7
4. Inverse method for the characterization of 2D-diffraction gratings	
<i>B. Trauter, K.-H. Brenner</i>	8
5. Polarization-independent photodetectors with enhanced responsivity in a standard Silicon-on-Insulator CMOS process	
<i>M. Auer, K.-H. Brenner</i>	9
6. Minimal realization of arbitrary optical systems defined by ray transfer matrices	
<i>X. Liu, K.-H. Brenner</i>	10
7. New method for rigorous simulation of local absorption in periodic structures	
<i>M. Auer, K.-H. Brenner</i>	11
8. Integrated beam splitters for parallel microscopy in life science	
<i>D. Wohlfeld, E. Slognat, K.-H. Brenner</i>	12

9. Efficient coupling using GRIN-rod lenses	
<i>F. Merchán, K.-H. Brenner</i>	13
10. Fabrication of integrated optical coupling structures	
<i>F. Merchán, K.-H. Brenner</i>	14
11. Non-stereoscopy method for deflectometric measurement of reflecting surfaces	
<i>E. Slogsnat, K.-H. Brenner</i>	15
12. Miniaturized parallel microscopy	
<i>E. Slogsnat, K.-H. Brenner</i>	16
13. Guiding structures for splicing single-mode fibres using deep UV lithography fabrication	
<i>X. Liu, K.-H. Brenner</i>	17

Full control of light intensity by beam shaping

K.-H. Brenner

Beam shaping is commonly used to transform a given intensity distribution into a different, desired intensity distribution. Applications of one-dimensional (rotationally symmetric) beam shaping [1,2] are typically in the area of high power lasers and optical illumination systems. Unlike one-dimensional beam-shaping, which leads to a simple differential equation, which can be integrated in a straight forward manner, the two-dimensional beam shaping problem leads to a nonlinear Monge-Ampere type equation, for which numerical solutions [3] are difficult to obtain. Recently, we have generalized the equations for optical beam shaping with two surfaces, derived a nonlinear Monge-Ampere type differential equation, which became solvable with the shifted-base-function (SBF) approach [4].

In an optical implementation, beam shaping can be realized by diffractive, by reflective or refractive optics. In fig. 1, we consider a refractive system in a telescopic geometry. The input medium and the output medium are assumed to have the same refractive index, here denoted by n_1 . The intermediate medium with a thickness of D on the optical axis has a refractive index of n_2 . The input and output coordinates are distinguished by small and large letters.

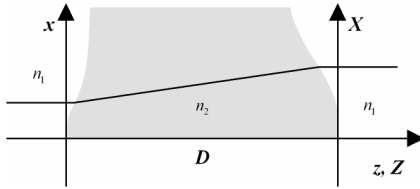


Fig. 1: Geometry for general two-dimensional beam shaping in a refractive telescopic arrangement.

Any beam shaping problem can be decomposed into a sequence of two tasks: 1) to find the mapping M of the input coordinates (x,y) to the output coordinates (X,Y) and 2) the calculation of the optical surfaces, required to achieve this task. With respect to the second task, we found an analytic expression for finding the surface z from the mapping M :

$$\begin{pmatrix} z_x \\ z_y \end{pmatrix} = \frac{1}{\sqrt{(v-1)^2 D^2 + (v^2-1)\Delta^2}} \begin{pmatrix} \Delta x(x,y) \\ \Delta y(x,y) \end{pmatrix} \quad (1)$$

This equation relates the beam shift $\Delta x = X - x$, $\Delta y = Y - y$ to the gradient of the front surface z . $v = n_1/n_2$ is the index ratio. The back surface Z can be determined uniquely using the constant path length condition. From the gradient, the surface can be determined easily by SBF-integration [4].

With respect to the first task, we use a far field approximation of eq. 1, which is sufficiently accurate, if the beam shift is small compared to the separation D , and express it in the form:

$$\nabla_{\perp} z \cong \frac{1}{|v-1|} \nabla S \quad (2)$$

With this, the beam shaping requirement can be expressed as a Monge-Ampere-type second order differential equation for S :

$$I_1(x + S_x, y + S_y) \cdot \left[(1 + S_{xx})(1 + S_{yy}) - S_{xy}^2 \right] = I_0(x, y) \quad (3)$$

It relates the second order partial derivatives of S to the input intensity I_0 and the desired output intensity I_1 . For solving this equation, we have developed a local optimization algorithm, which finds an acceptable numerical solution in less than 50 iterations.

As an example, we considered a Gaussian input illumination (fig 2, left) which is to be transformed into an image of the letter B. For verification, the result (fig. 2 right) was obtained by an independent calculation using Monte Carlo ray tracing through the surfaces z and Z .

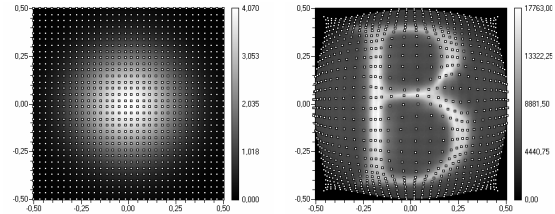


Fig. 2: left: Gaussian input distribution and reference positions of the SBF-approximation, right: Intensity obtained by Monte-Carlo ray trace with mapped positions

References:

- [1] F. Dickey and S. Holswade, *Laser Beam Shaping: Theory and Techniques* (Marcel Dekker, 2000).
- [2] D. L. Shealy, J. A. Hoffnagle, and K.-H. Brenner, *SPIE Proc.*, Vol. 6290, San Diego, 2006
- [3] J. Benamou and Y. Brenier, "A computational fluid mechanics solution to the Monge-Kantorovich mass transfer problem," *Numer. Math.* 84, 375–393 (2000).
- [4] K.-H. Brenner, *Journal of Physics: Conference Series* 139,01,2002, p. 11, Workshop on Information Optics (WIO'08), (2008)

Parallel image scanning with binary phase gratings

R. Buschlinger, K.-H. Brenner

Microscopy applications like in system biology or in industrial inspection generate an increasing demand for high-speed imaging techniques. An approach to satisfy this demand is spatial parallelization of the imaging system. In the case of wide-field imaging, the scan time depends on the ratio of lens diameter to field of view of each individual imaging system. To minimize the scan time, the number of lenses has to be maximized and therefore the size of the imaging systems has to be minimized.

Recently, we have developed a novel approach for parallel image scanning, whereby the intensity peaks are generated by a binary phase grating instead of a lens array. These binary phase gratings in a special configuration generate sharp spots for grating periods down to 3 wavelengths [1]. This was observed also experimentally.

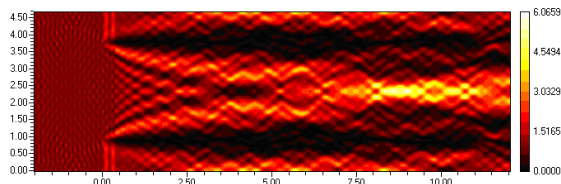


Fig. 1: Intensity in the x-z-plane behind a 2D-grating. Units are in microns

Compared to micro lenses, such gratings can be easily manufactured and enable a high degree of miniaturization

The diameter of the focal spot is not restricted by a numeric aperture according to Abbe's law and can be used to scan specimens with many spots simultaneously. Due to the high degree of parallelism, the imaging speed can be increased significantly.

In order to analyze, which grating configurations are practical for generating intensity patterns with distinct spots, the intensity on the optical axis was calculated for different z-positions and for a range of gratings with different fill factors using both, scalar diffraction theory and rigorous diffraction theory. A high intensity in the resulting plot is an indicator for the existence of a focal spot. With this method, optimum spot generation was predicted for fill factors, which lie on a straight line. Such a plot is shown in fig. 2. The horizontal axis shows the z-position in units of the Talbot length z_T . Due to symmetries, the plot is only shown for a quarter of the Talbot length. The vertical axis shows the fill factor ranging from zero to one. The light distribution clearly exhibits a fractal behaviour. For the focussing condition in fig. 1, we chose a fill factor of ~ 0.7 at a focussing distance of $\sim 0.12 z_T$. The absolute value of the grating period also plays an important role, since smaller periods reduce the number of propagating modes. As a

result, the plot in fig. 2 appears more blurred and the tolerances for fabrication a focusing grating are thus more relaxed. For smaller grating periods, we also observed an increase in effective numerical aperture, but also an increase of the bias amplitudes.

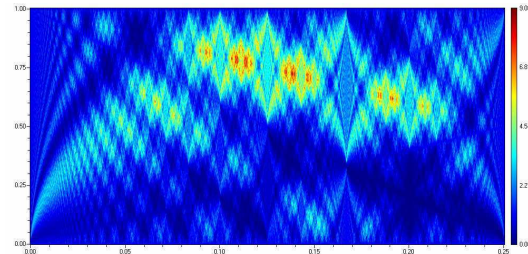


Fig. 2: left: Gaussian input distribution and reference positions of the SBF-approximation, right: Intensity obtained by Monte-Carlo ray trace with mapped positions

In an imaging application, only one spot plane should contribute to the detected information in each scanning step. If a specimen is placed inside one of the focal planes of a binary phase grating, its light transmission properties at the position of the spot can be measured in a detection plane behind the specimen. Figure 3 shows the result from a simulation using an absorber with a diameter of $1/8$ of the detector pixel size. The period of the grating, $P = 10\lambda$, matches the period of the detector array. The resolution obtained is approx. $1/5$ of the detector pixel size.

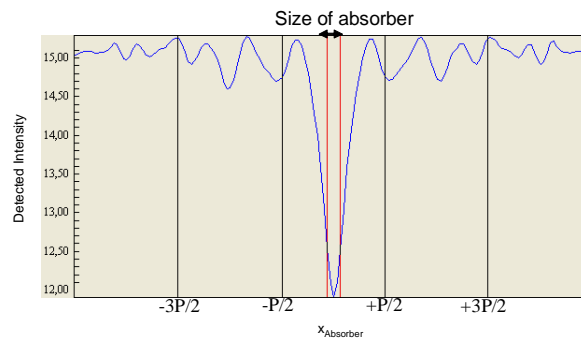


Fig. 3. Integrated detector intensity when an absorbing spot is scanned through the focal plane.

References:

- [1] R. Buschlinger, K.-H. Brenner, "Light Focusing by binary phase gratings", 5th EOS Topical Meeting on Advanced Imaging Techniques, Engelberg/Ch 2010 (AIT), ISBN 978-3-00-030503-0

Vector wave propagation method (VWPM) An extension to the wave propagation method

M. Fertig, K.-H. Brenner

We have extended the scalar wave propagation method (WPM) to vector fields. The WPM [1] has been introduced in 1993 in order to overcome the major limitations of the beam propagation method (BPM). The BPM is a paraxial light propagation method for the simulation of inhomogeneous media. Due to the paraxial approximation, its main application is in the simulation of wave guides. With the WPM, the range of applications could be extended from the simulation of waveguides to simulation of conventional optical elements like lenses and gratings. In [1] it was demonstrated that the (scalar) WPM provides valid results for propagation angles up to 85 degrees. Here, we extend the WPM to 3D vectorial fields by considering the polarization dependent Fresnel coefficients of amplitudes for transmission in each propagation step. Like in the WPM, we start with a plane wave expansion of the field at $z = 0$, which is the starting point at layer m

$$\tilde{\mathbf{E}}_{\perp,m}(\mathbf{k}_{\perp}) = \iint \mathbf{E}_{\perp,m}(\mathbf{r}_{\perp}) \cdot \exp(-i \mathbf{k}_{\perp} \mathbf{r}_{\perp}) d^2 \mathbf{r}_{\perp} \quad (1)$$

Unlike the WPM, we now consider the vectorial properties of the wave. The z -component is not needed for this step, since $\tilde{\mathbf{E}}_m(\mathbf{k}_{\perp})$ must satisfy the Maxwell equations. The transfer at the interface between layer m and $m+1$ is described by the Fresnel equations. These can be reformulated into a linear transformation

$$\tilde{\mathbf{E}}_{\perp,m+1}(\mathbf{k}_{\perp}) = \mathbf{M}_{m,m+1}(\mathbf{r}_{\perp}, \mathbf{k}_{\perp}) \cdot \tilde{\mathbf{E}}_{\perp,m}(\mathbf{k}_{\perp}) \quad (2)$$

The next step treats the propagation of a single plane wave component in an inhomogeneous layer

$$\tilde{\mathbf{E}}'_{\perp,m+1}(\mathbf{r}_{\perp}, \mathbf{k}_{\perp}) = \tilde{\mathbf{E}}_{\perp,m+1}(\mathbf{k}_{\perp}) \cdot \exp(i \phi_{m+1}(\mathbf{r}_{\perp}, \mathbf{k}_{\perp})) \quad (3)$$

Due to the inhomogeneity of the medium, the propagation phase is dependent on both, position and direction. In the final step, the propagated wave amplitudes are summed up.

$$\mathbf{E}_{m+1}(\mathbf{r}_{\perp}) = \iint \tilde{\mathbf{E}}'_{m+1}(\mathbf{r}_{\perp}, \mathbf{k}_{\perp}) \cdot \exp(i \mathbf{k}_{\perp} \mathbf{r}_{\perp}) \frac{d^2 \mathbf{k}_{\perp}}{(2\pi)^2} \quad (4)$$

For homogeneous media, this step has the form of a Fourier back-transformation. In the inhomogeneous case, however, $\tilde{\mathbf{E}}'_{\perp,m+1}(\mathbf{r}_{\perp}, \mathbf{k}_{\perp})$ is dependent also on position. Therefore, an inverse Fourier transformation cannot be applied. We verify the validity of this approach by transmission through a prism and by comparison with the focal distribution from vectorial Debye theory. The simulation provides the correct amplitudes and deflection angle according to electromagnetic theory.

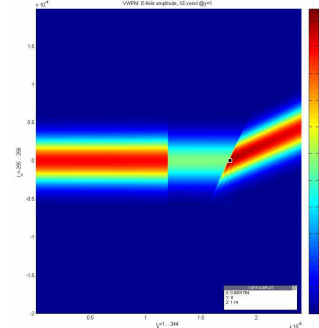
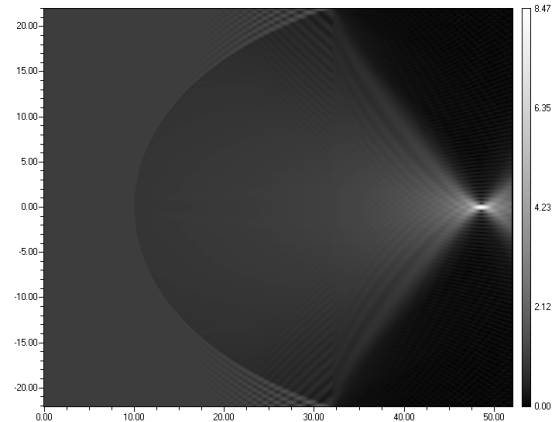


Fig. 1: Electric field intensity of a Gaussian beam propagating through a prism

Fig. 2 shows the amplitude distribution of a plane wave passing through an ideal focussing lens with a numeric aperture of 0.85. The focal distribution agrees perfectly with the results from vectorial Debye theory.



Unlike rigorous methods, which are only able to simulate small volumes, the VWPM, due to the decomposition into separate layers can also simulate much larger volumes and is therefore a suitable tool between the macroscopic and the microscopic world.

References:

- [1] K.-H. Brenner and W. Singer, "Light propagation through micro lenses: a new simulation method" *Applied Optics* 32, (1993), 4984.4988
- [2] M. Fertig, K.-H. Brenner, "The vector wave propagation method (VWPM)", *JOSA A*, Vol. 27, No. 4, pp. 709 – 717, (2010)

Inverse method for the characterization of 2D-diffraction gratings

B. Trauter, J. Hetzler, K.-H. Brenner*

Diffraction gratings are used in a wide range of applications. An accurate characterization is necessary to ensure a high quality of the element. Because grating periods decrease down to a few hundreds of nanometers, optical microscopy reaches its limits, if grating parameters like grating height or fill factor should be determined with high accuracy. Only methods like Atomic Force Microscopy or Scanning Electron Microscopy offer the necessary precision but also suffer from some disadvantages. We analyzed an inverse method which is similar to scatterometry, often used for the inspection of semiconductor structures. The method allows the determination of the grating parameters of a two-dimensional diffraction grating by measuring the diffraction efficiency of several diffraction orders. By use of a rigorous calculation method, we can numerically solve the inverse grating diffraction problem and determine the grating shape out of the diffraction orders.

Method	Resolution	Disadvantages
Microscope	100 nm	Resolution insufficient
AFM	10 nm	Non-optical method, Local method, Tip size limits 3D resolution
Electron Microscope	1 nm	Non-optical method, Local method, Grating needs to be prepared
Grating reconstruction	few nm	Indirect method No local measurement possible

Table 1: Comparison of different measurement techniques

The method is based on the comparison of measured and calculated diffraction efficiencies. Through minimizing the differences by means of an optimization algorithm, the grating parameters can be determined.

For the measurement the diffraction grating is being measured under different illumination settings (for example at different wavelengths). A detector determines the relative intensity (i.e. the diffraction efficiency) of a certain diffraction order.

On a Computer, the diffraction efficiencies for a certain grating model are being calculated. An optimization algorithm varies the grating parameters as long as the calculated efficiencies fit well to the measured ones. For the simulation of the grating the Rigorous Coupled Wave Analysis (RCWA) was used.

For a fast calculation of the iteration steps, we used an extension of the RCWA that directly provides the derivatives of the diffraction efficiency with respect to the grating parameters used for the optimization. [1,2]

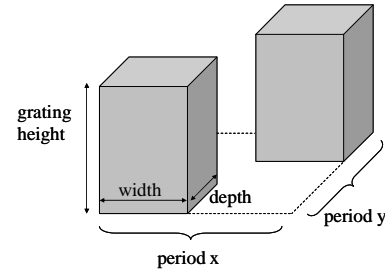
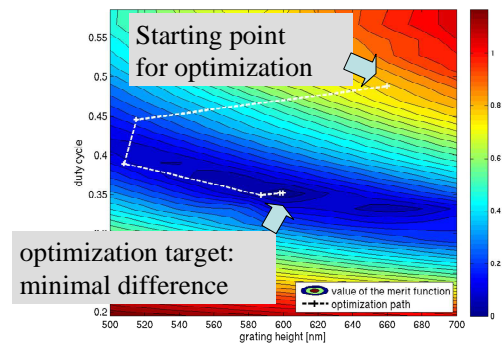


Fig. 1: Model parameters for the test case, a checkerboard pattern



Comparison	AFM	Reconstr.	Difference
Fill factor	0.45-0.5	0.47	6.4 %
Grating height	669 nm	665 nm	0.6 %

Table 2: Comparison of the results for the test case

Table 2 shows a comparison between AFM measurements and the grating reconstruction method for two different grating parameters, the fill factor and the grating height. The results are in good agreement and thus clearly demonstrate the validity of the method.

References:

- [1] N.P. Van der Aa, R.M.M. Mattheij, J. Opt. Soc. Am. A, Vol. 24, No. 9, p. 2692-2700 (2007).
- [2] B. Trauter, J. Hetzler, K.-H. Brenner, "Inverse method for the characterization of two-dimensional diffraction gratings", 14th Microoptics Conference, 25.-27.9., Brussels, Belgium, Technical Digest, pp 131 (2008).

* Carl-Zeiss SMT AG Oberkochen

Polarization-independent photodetectors with enhanced responsivity in a standard Silicon-on-Insulator Complementary Metal–Oxide–Semiconductor (CMOS) process

N. Moll*, T. Morf*, M. Fertig**, T. Stöferle*, B. Trauter, R. F. Mahrt*, J. Weiss*, T. Pflüger**, and K.-H. Brenner

Today, the realization of optical chip-to-chip communication is restricted by the challenges of combining optical detectors and light sources with integrated CMOS circuits. Although CMOS technologies already offer a wide range of intrinsic pn-junctions, that can be used to build a detector, the high doping levels of state-of-the-art technologies lead to very narrow depletion regions of approximately 50–100nm and very high junction capacitances, which severely limit the frequency response of such a detector. The small depletion regions also result in a very small responsivity because of the limited volume available to absorb photons and generate charge carriers.

In this work an optical detector in a silicon-on-insulator (SOI) CMOS process was implemented with an approximately 70–100-nm-thick active Si layer, where under normal conditions less than 5% of long wavelength light would be absorbed. In order to enhance the absorption, a resonant feedback structure was introduced to increase the effective interaction length.

The SOI CMOS technology already provides poly-Si gates in a grating structure, which can be utilized to provide the required feedback for a photodetector at a selected wavelength (cf. Fig. 1).

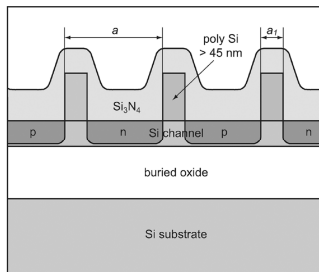


Fig. 1

Schematic cross section of the grating structure in a standard SOI CMOS process. The geometric parameters are the grating period a and the poly-Si gate width a_1 (in a metal–oxide–semiconductor field-effect transistor (MOSFET), this dimension is referred to as the gate length).

By applying a slight p-doping to the active Si channel and heavy n- and p-dopings to source and drain, we basically implemented the source-drain implant of a negative channel field effect transistor (FET), but with a switched polarity on one side. The result is a lateral p-i-n diode, where the depletion region forms under the poly gate.

The photodetector device works by inducing a standing wave inside the device when light couples to the second-order grating. The standing wave is then absorbed by generating electron-hole pairs in the depletion region under the gate, where an electric bias voltage is applied. Thereby an electric current is created between the n- and the p-well.

In order to optimize the design, we performed a 2D finite-difference time-domain (FDTD) simulations. These simulations of 1D gratings clarified, that in order to obtain a po-

larization independent resonance at 650nm, different gratings periods for s- and p-polarization are necessary [1] and thus no single 1D grating configuration is sufficient. Therefore we introduced corrugations perpendicular to the first grating to construct a polarization-independent grating. For unpolarized light, the total absorption is the average of the two absorption values. That way we achieved a total absorption of 59% for 650nm wavelength (cf. Fig. 2).

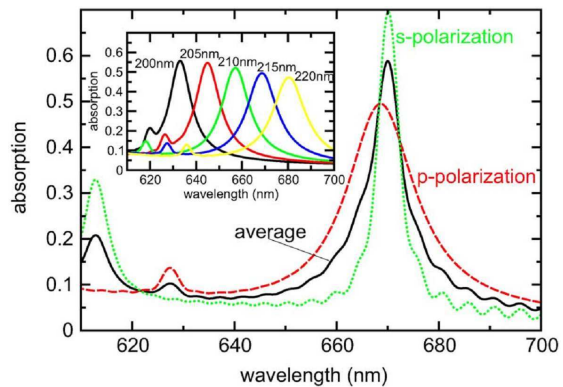


Fig. 3

Calculated absorption spectra of the 2D grating as a function of the wavelength for both the s- and p-polarization. The grating period a_{TM} is 215 nm, the gate width a_1 is 60 nm. The calculated absorption spectra are functions of the wavelength for five different grating periods. The other parameters are kept fixed.

The 1D and 2D photodetectors designed were fabricated in a standard 45-nm SOI CMOS process. For the characterization of the detectors, a mode-locked Ti-sapphire pulse laser was used as excitation light source. Further details of the experimental setup and results can be found in [1].

References:

- [1] N. Moll, T. Morf, M. Fertig, T. Stöferle, B. Trauter, R. F. Mahrt, J. Weiss, T. Pflüger, and K.-H. Brenner, *Polarization-Independent Photodetectors With Enhanced Responsivity in a Standard Silicon-on-Insulator Complementary Metal–Oxide–Semiconductor Process*, *J. Lightwave Technol.*, vol. 27, no. 21, 2009

* IBM Zürich

** IBM Böblingen

Minimal realization of arbitrary optical systems defined by ray transfer matrices

X. Liu, K.-H. Brenner

Optical systems can be described paraxially by ray transfer matrices that specify the relation between paraxial entrance rays and exit rays. In this research project, we consider the inverse problem: a desired optical system is given by the ray transfer matrix, and by means of the matrix decomposition we look for the minimal optical realization that consists of only lenses and pieces of free-space propagation.

Summarized and outlined in book [1], similar decompositions have been studied before but without a restriction to these two elements types - lens and propagation, also without an attempt for minimization. As the main results of this research, general one-dimensional (1D) optical systems can be synthesized with a maximum of four elements and two-dimensional (2D) optical systems can be synthesized with six elements at most.

One-Dimensional Optical Systems

Any 1D optical system can be described by a 2x2 symplectic matrix $\mathbf{M} = \begin{pmatrix} A & B \\ C & D \end{pmatrix}$. The two primary elements, lens and propagation over a positive distance, exhibit the ray matrices \mathbf{L} and \mathbf{P} respectively as following

$$\mathbf{L}(f) = \begin{pmatrix} 1 & 0 \\ -1/f & 1 \end{pmatrix}, \quad \mathbf{P}(z > 0) = \begin{pmatrix} 1 & z \\ 0 & 1 \end{pmatrix},$$

where f denotes focal length and z is positive propagation distance.

The coordinate inversion matrix $\Psi(\pi) = -\mathbf{I}$ is introduced as an auxiliary element in the decomposition. Its presence does not increase the complexity of the optical system. It will be located, if present, only at the entrance or exit side of systems, which means a 180° rotation of the object or the optical detector. Following are the minimal decompositions for 1D systems:

- $B > 0$: **LPL**. If $A = 1$ (or / and $D = 1$), the right (or / and left) lens can be omitted.
- $B < 0$: $\Psi(\pi)$ **LPL**. If $A = -1$ (or / and $D = -1$), the right (or / and left) lens can be omitted.
- $B = 0$ $A = D = 1$ or -1 : **L** or $\Psi(\pi)$ **L**
- $B = 0$ $A \neq D$ $A > 0$ $C > 0$: **PLP**
- $B = 0$ $A \neq D$ $A > 0$ $C > 0$: $\Psi(\pi)$ **PLP**
- $B = 0$ $A \neq D$ $A < 0$ $C \geq 0$: **PLPL** or **LPLP**
- $B = 0$ $A \neq D$ $A > 0$ $C \leq 0$: $\Psi(\pi)$ **PLPL** or $\Psi(\pi)$ **LPLP**

The maximal cases include 4 primary elements.

Two-Dimensional Optical Systems

Any 2D optical system can be described by a 4x4 symplectic matrix $\mathbf{M} = \begin{pmatrix} \mathbf{A} & \mathbf{B} \\ \mathbf{C} & \mathbf{D} \end{pmatrix}$ with $\mathbf{A}^T \mathbf{C} = \mathbf{C}^T \mathbf{A}$, $\mathbf{B}^T \mathbf{D} = \mathbf{D}^T \mathbf{B}$, and

$\mathbf{A}\mathbf{D}^T - \mathbf{B}\mathbf{C}^T = \mathbf{I}$, where \mathbf{A} , \mathbf{B} , \mathbf{C} , \mathbf{D} are 2x2 block matrices and \mathbf{I} is the identity matrix. The two primary elements, astigmatic lens and isotropic propagation over a positive distance, exhibit the ray matrices \mathbf{L} and \mathbf{P} respectively as following

$$\mathbf{L}(f_x, f_y) = \begin{pmatrix} 1 & 0 & 0 & 0 \\ 0 & 1 & 0 & 0 \\ -\frac{1}{f_x} & 0 & 1 & 0 \\ 0 & -\frac{1}{f_y} & 0 & 1 \end{pmatrix}, \quad \mathbf{P}(z > 0) = \begin{pmatrix} 1 & 0 & z & 0 \\ 0 & 1 & 0 & z \\ 0 & 0 & 1 & 0 \\ 0 & 0 & 0 & 1 \end{pmatrix},$$

where f_x and f_y denote focal lengths and z is positive propagation distance.

Coordinate rotation in the lateral plane corresponds to

$$\mathbf{R}(\varphi) = \begin{pmatrix} \cos \varphi & \sin \varphi & 0 & 0 \\ -\sin \varphi & \cos \varphi & 0 & 0 \\ 0 & 0 & \cos \varphi & \sin \varphi \\ 0 & 0 & -\sin \varphi & \cos \varphi \end{pmatrix},$$

which is an additional auxiliary element. Its multiple presence does not increase the complexity of the optical system since it can be implemented practically by rotating the subsequent optical element.

To determine the optical minimal decomposition, we distinguish between two cases:

- $|\mathbf{B}| \neq 0$: a maximum of five optical elements (lens and propagation) is sufficient for a realization of this matrix type: **RLRPLPRLR**.
- $|\mathbf{B}| = 0$: a maximum of six optical elements (lens and propagation) is sufficient for a realization of this matrix type: **RLRPLPRLRP**.

Decomposition of 2D systems thus consists of a maximum of six primary elements.

References:

- [1] Wolf, K. B.; "Geometric Optics on Phase Space", Springer, 2004
- [2] Liu, X.; Brenner, K.-H.; „Minimal optical decomposition of ray transfer matrices”, Appl. Opt. **47**, E88-E98, 2008

New method for rigorous simulation of local absorption in periodic structures

M. Auer, K.-H. Brenner

For computer-aided optimization of lithography, photo-detectors and photovoltaic elements, precise mathematical models of the underlying physical absorption processes are indispensable. Nevertheless, in most cases, the standard tools for optimization of light efficiency in photo-sensitive materials only consider the intensity distribution in these devices. In the context of lithography, for example, the resist exposure is proportional to the amount of energy, which is absorbed in a finite volume element. In photodetector design, the location of photon-electron generation plays an important role for the responsivity of the photodiode, because only those electrons, which are generated near the depletion region, contribute to the photocurrent, while electrons generated in other regions mostly contribute to local heating.

Starting with Poynting's theorem, one can derive a formula for the quantitative calculation of the ratio of absorbed power to incident power in a volume element (V) for an illumination with a plane wave according to:

$$\frac{P_a}{P_i} = \frac{k_0^2}{k_{i,z}} \cdot \frac{1}{A} \cdot \iiint_V \text{Im}(\epsilon(\mathbf{r})) \cdot |\mathbf{E}_1(\mathbf{r})|^2 dV \quad (1)$$

The absorbed power thus depends on the imaginary part of the permittivity $\text{Im}(\epsilon(\mathbf{r}))$ at location \mathbf{r} . k_0 and $k_{i,z}$ refer to the vacuum wave number and the z -component of the wave vector of the incident wave, exposing an area A . \mathbf{E}_1 refers to the electric field response inside the material to an incident field with unit amplitude. Using the "Rigorous Coupled Wave Analysis" (RCWA), a standard method for the calculation of diffraction efficiencies, the near-field distribution \mathbf{E}_1 does not provide the correct absorption values in the case of TM-polarization. By modifying the field definitions, taking mode truncation into account, we have achieved perfect agreement between global absorption and integrated local absorption[1]

Based on this result, we also developed a new concept for a SOI-CMOS-compatible photodetector [2]. Using this technology for photo detection, there are many problems to deal with: Ultra thin layers limit the height (about 70nm) of the active zone. High doping levels cause narrow depletion regions. The assortment of materials is rather limited. Furthermore, for wavelengths above 850nm, Silicon is almost transparent.

Our approach utilizes the poly-silicon layer, which usually forms the transistor gates, as a resonant grating to concentrate the incident light inside the depletion region (cf.

Fig.1-a,d). Unlike other approaches using Fabry-Perot resonances or surface plasmon resonances, our approach utilizes **lateral resonances**.

In a simulation, grating period and gate width form a two-dimensional parameter space, which can be scanned **layerwise** for absorption maxima (cf. Fig.1-b,c). By realizing a grating with a suitable combination of design parameters, we have optimized our design to an absorption level of 68.4% in the active channel - in contrast to 2.18% absorption obtained without optimization. This corresponds to an increase of efficiency by a factor of 31, while staying fully CMOS-compatible without any need for additional post processing steps.

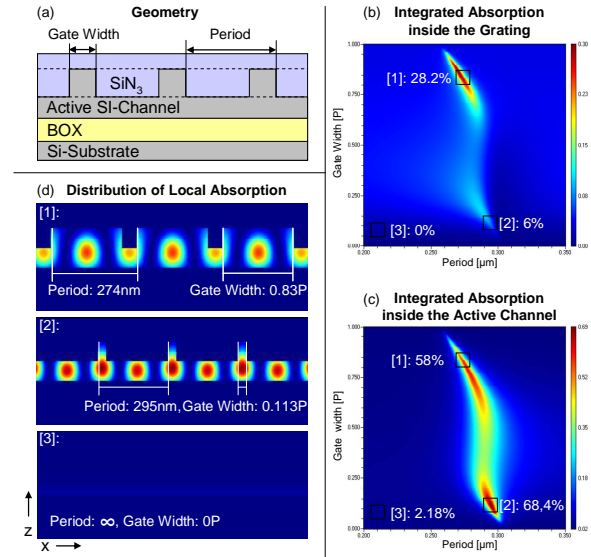


Fig. 1:

(Polarisation: TE, Wavelength: 850nm)

- Geometry of the layer stack and the simulation parameters (a).
- Integrated absorption of the grating layer (b) and the active layer (c) for a wide range of gate width and period values.
- Distribution of local absorption inside the layer stack for three parameter combinations (d).

References:

- [1] Brenner, K.-H. Optics Express, Vol. 18, Issue 10, pp. 10369-10376 (2010)
- [2] M. Auer, K.-H. Brenner, N. Moll, T. Morf, M. Fertig, T. Stöferle, R.F. Mahrt, J. Weiss, T. Pflüger, EOS Topical Meeting on Diffractive Optics, Koli/Finland, ISBN 978-3-00-024193-2, (2010)

Integrated beam splitters for parallel microscopy in life science

D. Wohlfeld, E. Slogsnat, K.-H. Brenner

High-throughput fluorescence-microscopy is used by biologists to define and model gene functions on a genome-wide scale. Besides high spatial resolution, the imaging speed, especially in time-sequence imaging, is an important factor. A significant increase in scan speed can be achieved by parallelization. The parallelism of microscopy is limited by the size of one imaging system and the ratio between lens diameter (D) and field of view (FoV) of the objectives. Thus miniaturization enables a higher degree of parallelism.

	Classic parallel	Micro lens system	GRIN-rod lens system
Magnification	10	6.1	4.6
NA	0.4	0.35	0.35
Resolution	~ 1 μm	~ 1 μm	~ 1 μm
Chromatic aberration correction	yes	no	no
Lens diameter	28 mm	1.2 mm	2 mm
Field of View	2600 μm	120 μm	400 μm
Scans for total plane	12	10	5
Scans to cover spots	12	8	3

Table 1: Comparison of classic and miniaturized parallel microscopy

Furthermore, aberrations scale down with the lens size. The maximum degree of parallelism can be achieved ideally, if the ratio of FoV/D is one. Table 1 shows a comparison between a classic fluorescence objective, a micro lens array approach and a GRIN-rod lens system [1].

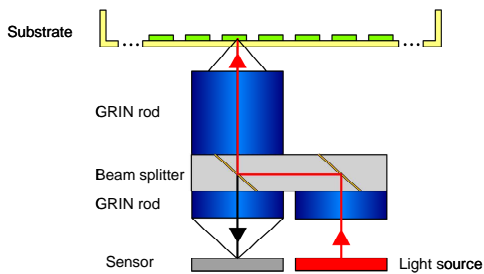


Fig. 1: GRIN-lens approach for fluorescence microscopy. The imaging and illumination paths are separated by a beam splitter.

Fig. 1 depicts an illustration of the micro-integrated parallel microscope system. In the top layer are the front imaging lenses, the intermediate layer consists of beam splitters and in the bottom layer the collimation lenses and the imaging lenses are mounted.

The GRIN-rod lens system from table 1 was designed by optimizing the length of available GRIN-rod lenses and the parameter n_4 of the index distribution using a Zemax simulation.

The beam splitters were replicated with a UV-curable polymer from a negative metal master fabricated by micro-diamond turning at the LFM in Bremen. The master and the replication are shown in figure 2 and 3.

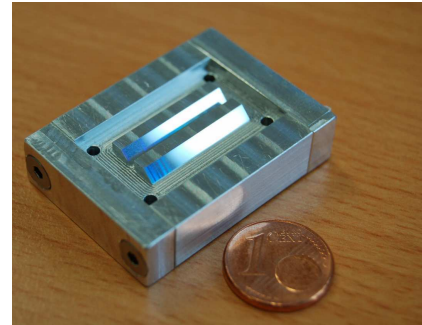


Fig. 2: Metal master for fabrication of the beam splitters.

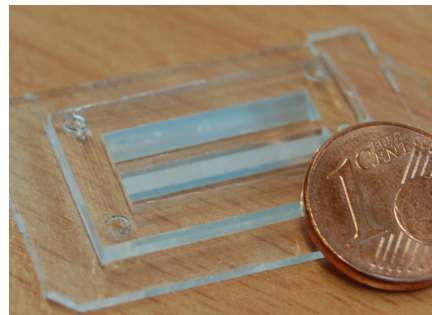


Fig. 3: Replication in a transparent polymer

References:

- [1] D.Wohlfeld, E. Slogsnat, K.-H. Brenner: „Integrated beam splitters for array microscopy in life science“ DGoO-Proceedings, ISSN: 1614-8436, 110. 2009, Brescia, Italy

Efficient coupling using GRIN-rod lenses

F. Merchán, K.-H. Brenner

In optical communication systems the key factor for assuring a high signal quality is the light efficiency of the coupling system. The divergent beam coming from a VCSEL has to be coupled into the optical fiber at the sender side and for the receiver the beam coming from the optical fiber has to be coupled into the photodiode. In order to collect the divergent light we proposed the use of a GRIN-rod lens [1]. We compared mathematical models, simulations and laboratory experiments in order to confirm the increment of coupling efficiency when using this device in a coupling system.

For the description of the GRIN lens the paraxial approximation of the ABCD Matrix was used in which a perfect imaging can be achieved, when the working distances fulfill the following equation:

$$\text{atan}\left(d_2\sqrt{-2n_0n_{r2}}\right) + \text{atan}\left(d_1\sqrt{-2n_0n_{r2}}\right) + \frac{L}{n_0}\sqrt{-2n_0n_{r2}} = \pi$$

which is valid for a parabolic index profile of the form

$$n(r) = n_0 + n_{r2}r^2$$

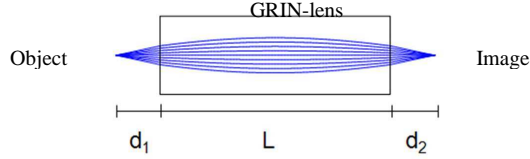


Fig. 1: Imaging through a GRIN lens.

We use the Sellmeier formula in order to treat dispersion

$$n_{z\text{emax}}^2(\lambda, r) = n_{ref}^2(r) + K_1(r) \cdot \left(1 - \frac{\lambda_{ref}^2}{\lambda^2}\right)$$

$$\begin{cases} n_{ref}(r) = n_0 + n_{r2} \cdot r^2 + n_{r4} \cdot r^4 \\ K_1(r) = K_{11} + K_{13} \cdot n_{ref}^2(r) \end{cases}$$

that can be developed in a power series as follows

$$n_{fit}(\lambda, r) = n_0(\lambda) + n_{r2}(\lambda) \cdot r^2$$

$$\begin{cases} n_0(\lambda) = \sqrt{n_0^2 + (K_{11} + K_{13}n_0^2) \frac{\lambda^2 - \lambda_{ref}^2}{\lambda^2}} \\ n_{r2}(\lambda) = \frac{n_0n_{r2}}{n_0(\lambda)} \left(1 + K_{13} \frac{\lambda^2 - \lambda_{ref}^2}{\lambda^2}\right) \end{cases}$$

The theoretical model was compared to experimental results. The setup of fig. 2 was used to evaluate the image definition and some statistical measures like FWHM (Full Width at Half Maximum) of intensity distributions at different work distances.

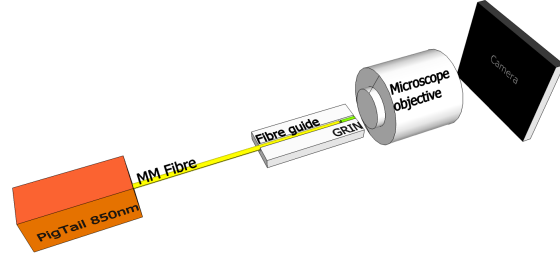


Fig. 2: Sketch of the first setup for verification of the GRIN imaging characteristics

In the fig. 3 some images of the end surfaces of GRIN lens and imaged fiber end surface are shown

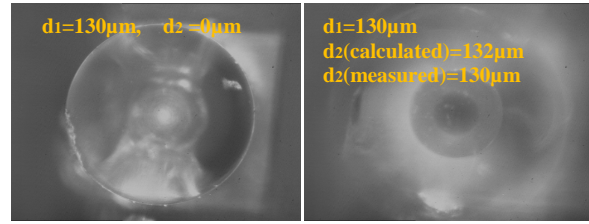


Fig. 3: End Surface of the GRIN rod (left) and of the fiber (right) The fig. 4 shows that the results predicted by theory and those obtained in practice are in good agreement.

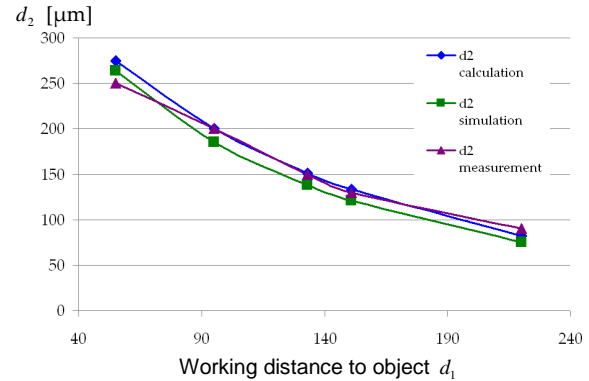


Fig. 4: comparison of calculation, simulation and measurement

The coupling efficiency was considerably increased by using a GRIN-rod lens.

References:

[1] F. Merchán, X. Liu, K.-H. Brenner, "Effiziente Faserkopplung mit Gradientenindex-Stablinen", DGaO-Proceedings (Online-Zeitschrift der Deutschen Gesellschaft für angewandte Optik e. V.), ISSN: 1614-8436, 111. Jahrestagung in Wetzlar, (2010)

Fabrication of integrated optical coupling structures

F. Merchán, K.-H. Brenner

High speed short-range interconnects have become a multidisciplinary research since the data links consist not only of electrical- but also of optical components. This combination offers at first, a utilization of the advantages of optics over electronics for signal transmission such as lower energy, lower noise-figure and light-weight cables and second, it also offers the advantages of electrical connectors like simplification of the handling, which is often difficult with optical connectors.

The research in this project is based on the design [1], integration and fabrication [2] of optical micro-couplers and the design of the electronic systems used for the test of the optical systems. The optical system is shown in figure 1. The coupler integrates mechanical systems like the funnel, the guide and the spacer; optical systems like the fiber, the (Gradient Index) GRIN-Lens and the mirror; and the optoelectronic components, in this case a VCSEL with the correspondent electrical connections.

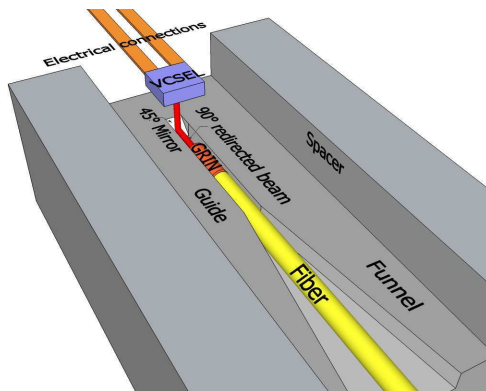


Fig. 1: 3D model of the optical system used to couple light from a VCSEL into a multi-mode fiber.

The optical micro-coupler is fabricated using plastic replication of metal masters. The metal masters are fabricated using a High-Speed-Cutting (HSC) machine for the shape and a robot lapping for the finish of the optical surfaces. The masters were manufactured with an accuracy of about 1 μ m and the surfaces had a roughness of about 10 nm after polishing.

In order to increase the coupling efficiency, a GRIN-lens can be introduced into the coupling system. The imaging properties of GRIN-lenses have been studied and characterized. One of the most relevant results is shown in figure 3. There, the comparison between two systems with and without GRIN-lens shows the advantages of using a

GRIN-lens when the working distance between the VCSEL and the fiber is above 70 μ m.

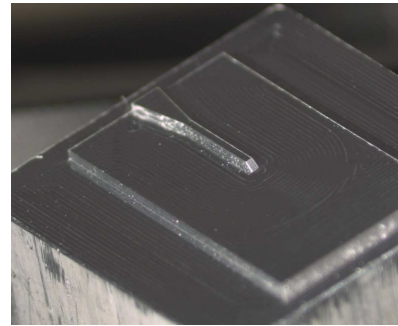


Fig. 2: Fabricated single channel metal-master

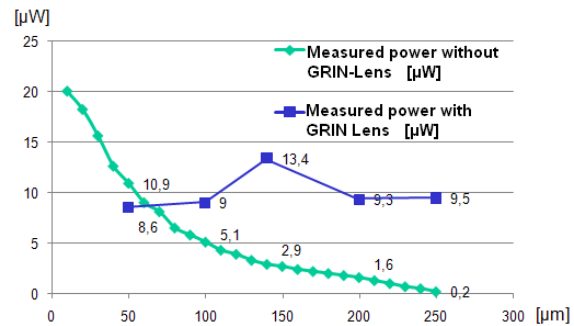


Fig. 3: Comparison of coupled power for two systems: with and without GRIN-lens

References:

- [1] F. Merchán, D. Wohlfeld, K.-H. Brenner, "Micro integration of optical components for the fabrication of active optical cables", Journal of the European Optical Society - Rapid Publications, Vol. 5, Pub.nr. 10056 (2010)
- [2] F. Merchán, K.-H. Brenner, R. Bórret, U. Berger, „Cost optimized fabrication of Micro-Optical Couplers“, Optical Fabrication and Testing (OF&T), OSA, Technical Digest, ISBN 978-1-55752-893-3, 13.-16-06.2010, Jackson Hole, Wyoming, USA, (2010)
- [3] F. Merchan, X. Liu, K.-H. Brenner, "Effiziente Faserkopplung mit Gradientenindex-Stablinen", DGaO-Proceedings (Online-Zeitschrift der Deutschen Gesellschaft für angewandte Optik e. V.), ISSN: 1614-8436, 111. Jahrestagung in Wetzlar, (2010)

Non-stereoscopic method for deflectometric measurement of reflecting surfaces

E. Slogsnat, K.-H. Brenner

Introduction

In systems biology there is a demand for accelerated image acquisition, especially when performing genome-wide screens.

In this research project a method was developed to eliminate the focus search, which is the most time-critical factor. Focussing is needed, when different positions on a substrate are examined. The refocusing is necessary due to the deformations of the glass substrates used in microscopy. These are 50- to 100-times larger than the depth of field. By eliminating the focusing step, the data throughput is enhanced significantly.

Ambiguity of surface normal determination

Deflectometry is used to determine the height deviations of the glass layer. In deflectometry, the slopes of the surface can be measured by observing a regular pattern, reflected from the glass surface.

General deflectometric methods are subject to an ambiguity regarding the determination of the surface normals. Assuming that the position of one point in the pattern is found in the sensor plane, the corresponding camera ray can be calculated directly. Back tracking this ray yields many possible surfaces – and therefore normals – which reflect the pattern point into the camera.

This approach uses a priori information about the surface and an iterative algorithm to resolve this ambiguity.

Non-stereoscopic surface reconstruction

It is assumed that the surface has a smooth height distribution without discontinuities and that its borders lie on a holding frame (Fig. 1).

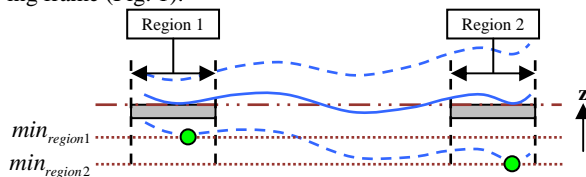


Fig. 1: Original surface lying on a frame and two reconstructed surfaces with wrong start heights

A self-consistent iterative method is used to reconstruct a surface corresponding to a given start height. The height values are approximated from gradient data by shifted base functions.

The first reconstruction is done with an arbitrary start height. If the start height does not match the correct one the reconstructed surface shows a slight deformation and – importantly here – a characteristic tilt (Fig. 1).

The tilt is visible in the difference between the minima in the surface's frame regions:

$$\Delta h_{\min} = \min_{\text{region1}} - \min_{\text{region2}}$$

If the absolute value of Δh_{\min} is equal or below a given threshold, the algorithm stops and the height distribution of the measured surface is obtained with high accuracy.

In the other case, the sign of Δh_{\min} defines the direction in which the start height has to be altered. If Δh_{\min} is positive, the start height has to be increased, if Δh_{\min} is negative the start height has to be decreased. The step size is decreased, if a change in the direction occurs. Then another reconstruction with the new value is performed.

Fig. 2 shows the reconstruction result for a simulated height distribution.

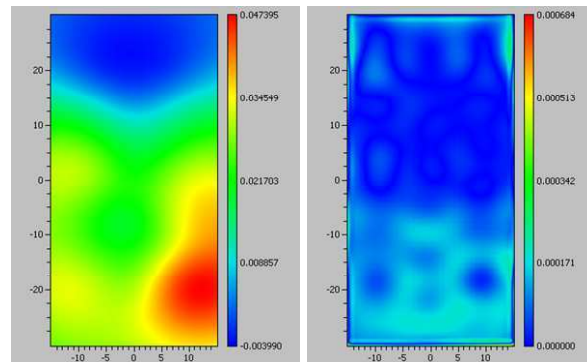


Fig. 2: Reconstructed height distribution and absolute value of the difference between reconstructed and simulated height distribution (units: mm)

Publications:

[1] E. Slogsnat, K.-H. Brenner, P. Ehrle, W. Stumpfs, "Selbstkonsistentes iteratives Verfahren zur Bestimmung glatter Oberflächen", DGaO-Proceedings (Online-Zeitschrift der Deutschen Gesellschaft für angewandte Optik e. V.), ISSN: 1614-8436, 109. Jahrestagung in Esslingen am Neckar/Deutschland (2008)

[2] E. Slogsnat, K.-H. Brenner, "Non-stereoscopic method for deflectometric measurement of reflecting surfaces", DGaO-Proceedings (Online-Zeitschrift der Deutschen Gesellschaft für angewandte Optik e. V.), ISSN: 1614-8436, 110. Jahrestagung in Brescia/Italien, (2009)

Miniaturized parallel microscopy

E. Slognat, K.-H. Brenner

Introduction

When performing genome-wide screens in systems biology, a large number of single experiments is observed with fluorescence-microscopy. Typically automated wide-field microscopes are used for this task.

To accelerate the image acquisition, an optical system for a miniaturized parallel fluorescence-microscope was designed.

Parallelization

The ratio of lens diameter to field of view (D_l/FOV) is a limiting factor for the parallelization. In addition to the degree of parallelization N_{scan} , the scan distance d_{scan} and the velocity v_{scan} , the scanning time T primarily depends on this factor:

$$T = \frac{D_l}{FOV} \frac{1}{N_{scan}} \frac{d_{scan}}{v_{scan}}$$

Scaling of an Optical System

When scaling an optical system down, the off-axis aberrations are also scaled, which is advantageous regarding the FOV .

It can be shown, that an advantageous ratio D_l/FOV is reached by scaling down the system (scaling factor $s < 1$). Additionally the parallelization in the scan direction can be used more efficiently.

Then the following relationship applies for the scan time T :

$$T \sim s\sqrt{s}$$

Conceptual Design

The optical system consists of three layers: To guide the excitation light to the object, a beamsplitter layer resides between two GRIN-lens arrays, which are fixed on glass substrates (Fig. 1).

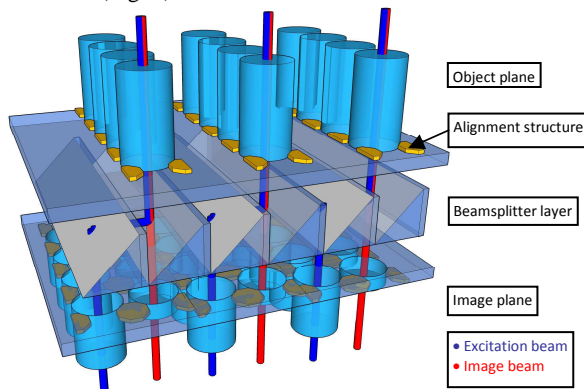


Fig. 1: Integration scheme of the miniaturized parallel fluorescence-microscope

Demonstrator

To analyze the image quality and the assembly of the layers, a demonstrator for the imaging path was set up (Fig. 2 and Fig. 3).

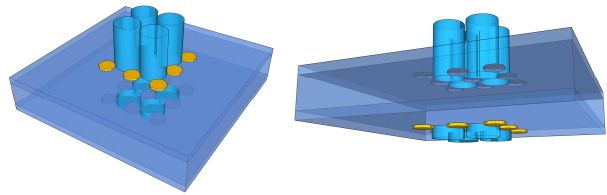


Fig. 2: Sketch of the optical demonstrator system.



Fig. 3: Left: SU-8 mounting structure; Middle: GRIN-lenses on the image side; Right: GRIN-lenses on the object side

The optical system was optimized for use with the fluorophore DAPI. The assembled demonstrator consists of four parallel optical channels with an NA of 0.44, a magnification of 4.29, a field of view of 400 μm and a lens diameter of 2 mm. With this system 125 line pairs/mm were resolved precisely (Fig. 4).

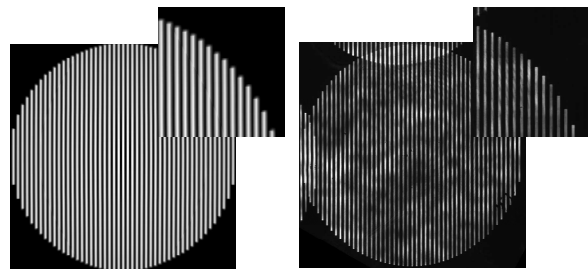


Fig. 4: 125 line pairs/mm (Left: simulation, Right: demonstrator)

References:

- [1] E. Slognat, R. Buschlinger, K.-H. Brenner, Miniaturisierte parallele Mikroskopie in der Systembiologie", DGaO-Proceedings, ISSN: 1614-8436, 111. Jahrestagung in Wetzlar (2010)

Guiding structures for splicing single-mode fibres using deep UV lithography fabrication

X. Liu, K.-H. Brenner

Optical fibres are used in a range of data communication applications, such as Wide Area Networks, Fibre-to-the-Home, Rack-to-rack interconnects. Since single-mode (SM) fibres can realize the transmission of broadband signals, a cost-efficient coupling method for SM fibres becomes increasingly important. The splicing method introduced here is executable with standard instruments. The splicing procedure is simple and quick. The transmission loss, however, resembles values achievable through the conventional thermal splicing, requiring trained personnel with special equipment.

Deep lithography is used here for the fabrication of a precise guide structure for aligning SM fibres. During splicing, the fibre ends are aligned precisely in the guide structure. Figure 1 shows the layout of the guide structure. The slight tapering (figure 1a) allows easy insertion of the fibres. The narrowing of the guide channel toward the substrate surface (figure 1b) guarantees that the fibres are clamped to the substrate. To minimize angular misalignment the guide structure is 6 mm in length. It is divided into several sub-segments to reduce stress induced by thermal expansion. By a replication processes, these guide structures can be fabricated cost-efficiently and precisely in large numbers.

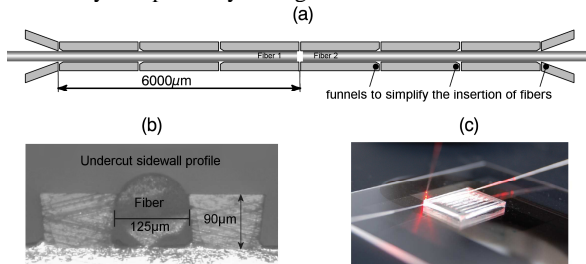


Fig. 1: (a) Layout of the guide structures, each with a length of 6mm. (b) An undercut sidewall profile. (c) A set of guide structures with coupling fibres inserted.

The lithographic process comprises the following steps: substrate cleaning and dehydrating, photo resist spinning, pre-bake, exposure, post-exposure bake and development. A detailed description with initial parameters can be found in [1]. In prior experiments, the guide structures were successfully implemented in the construction of a fibre resonator on a so-called “Atom Chip”. Calculated from the measured finesse of the resonator, a transmission loss of 0.013dB was achieved in the experiment [1].

In our experiments, a negative copy of a master from a lithographic process was formed in a thermally cured polymer, PDMS. This copy was then used as master in the next UV replication process. The PDMS stamp can be used more than 50 times and remains useable over several months. From the negative PDMS stamp a positive copy was subse-

quently formed in a UV curable polymer. This is the final guide structure that was used for splicing. A detailed description of thermal and UV replication with initial parameters can be found in [2]. Before the splicing procedure, SM fibres were polished to attain clean fibre ends. The fibres were then inserted into the channel until they “touch” each other in the middle of channel, whereupon a drop of UV adhesive is applied and subsequently cured by exposure under a UV light. The undercut sidewall profile clamps the fibres and ensures their position with a lateral misalignment smaller than 0.5µm. Despite the small tolerances, the fibres can be moved by hand longitudinally inside the channel and can be freely manoeuvred in proximity to each other up to a separation distance of 5µm.

In the splicing procedure, a small gap between the fibre ends is bridged with UV adhesive polymer. The loss caused by mismatch-induced reflection can be estimated from the refractive indices (figure 2 left). Another contribution to the transmission loss originates from divergence of the beam in the gap between the fibre ends. This loss can be calculated by use of the overlap integral (figure 2 middle). A significant contribution to transmission loss is caused by lateral misalignment of the fibre cores. It can result from imperfect centring during manufacture and also from improper alignment of the fibres during the splicing procedure. This loss can also be determined by the overlap integral (figure 2 right).

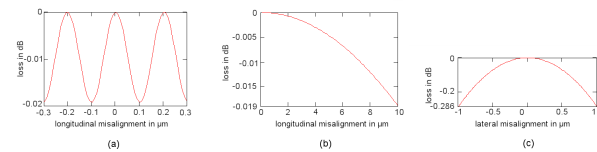


Fig. 2: Transmission loss through multiple reflection (left), divergence loss (middle) and loss caused by decentring (right). The wavelength assumed for the calculation was 650nm.

To analyse the coupling efficiency, two 5m SM fibres were bonded. Figure 3 illustrates the measurement setup. The net loss caused only by splicing amounted to 0.144dB.

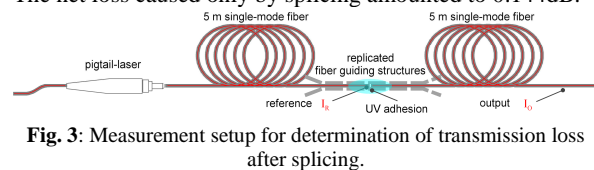


Fig. 3: Measurement setup for determination of transmission loss after splicing.

References:

- [1] X. Liu, K.-H. Brenner, M. Wilzbach, M. Schwarz, T. Fernholz and J. Schmiedmayer, *Appl. Opt.* **44**, 6875 (2005)
- [2] X. Liu and K.-H. Brenner, *Photonik*, Heft: 5/2008, 52 (2008)

Publications

1. Xiyuan Liu, Christian Hruscha, and Karl-Heinz Brenner, „Efficient reconstruction of two dimensional complex amplitudes utilizing the redundancy of the ambiguity function“, *Appl. Opt.* **47**, No. 22, pp E1 – E7 (2008)
2. Xiyuan Liu and Karl-Heinz Brenner, “Minimal optical decomposition of ray transfer matrices, *Appl. Opt.* **47**, No. 22, pp E88 – E98 (2008)
3. Andreas Unger, Karl-Heinz Brenner, “Vergleich exakter optischer Lösungsmethoden im Zeitbereich in Hinblick auf Genauigkeit und Effizienz“, *DGaO-Proceedings 2008*, <http://www.dgao-proceedings.de>, ISSN 1614-8436, 109. Jahrestagung in Esslingen am Neckar/Deutschland (2008)
4. Bastian Trauter, Karl-Heinz Brenner, “Schnelle Profilformbestimmung von diffraktiven Elementen durch Least-Square-Approximation mit verschobenen Basisfunktionen“, *DGaO-Proceedings 2008*, <http://www.dgao-proceedings.de>, ISSN 1614-8436, 109. Jahrestagung in Esslingen am Neckar/Deutschland (2008)
5. Ulrike Maier, Jens Hoffmann, Karl-Heinz Brenner, “Surface Reconstruction from gradient data“, *DGaO-Proceedings 2008*, <http://www.dgao-proceedings.de>, ISSN 1614-8436, 109. Jahrestagung in Esslingen am Neckar/Deutschland (2008)
6. E. Slogsnat, K.-H. Brenner, P. Ehrle, W. Stumpfs, “Selbstkonsistentes iteratives Verfahren zur Bestimmung glatter Oberflächen“, *DGaO-Proceedings* (Online-Zeitschrift der Deutschen Gesellschaft für angewandte Optik e. V.), ISSN: 1614-8436, 109. Jahrestagung in Esslingen am Neckar/Deutschland (2008)
7. INVITED: Karl-Heinz Brenner “Shifted Base Functions: An Efficient and Versatile New Tool in Optics“, *Journal of Physics: Conference Series* **139** 012002, 11 pp, ISSN 1742-6588, Workshop on Information Optics (WIO’08), 01.-05.06.08 in Annecy (2008)
8. B. Trauter, J. Hetzler, K.-H. Brenner, "Analysis of the uniqueness of an inverse grating characterization method", *Optics+Photonics*, 12.-14.8.2008, San Diego, USA, *Proceedings of the SPIE*, Vol. 7065 (2008)

9. B. Trauter, J. Hetzler, K.-H. Brenner, "Inverse method for the characterization of two-dimensional diffraction gratings", 14th Microoptics Conference, 25.-27.9., Brussels, Belgium, *Technical Digest*, pp 131 – 132 (2008)
10. Xiyuan Liu, Karl-Heinz Brenner, "Tiefenlithographie zum Spleißen von Singlemodefasern", *Photonik*, **40.** Jahrgang, No. 5, pp. 52-54 (2008)
11. N. Moll, T. Morf, M. Fertig, T. Stöferle, B. Trauter, R.F. Mahrt, J. Weiss, T. Pflüger, and K.-H. Brenner „Polarization-Independent Photo- Detectors with Enhanced Responsivity in a Standard SOI CMOS Process“, *IEEE Journal of Lightwave Technology*, Vol. **27**, No. 21, 4892-4896, (2009))
12. F. Merchán, D.Wohlfeld, K.-H. Brenner, " Development of active optical cables", Workshop of Optics in Computing (Optik in der Rechentechnik, ORT), *Proceedings of the Workshop Optics in Computing 2009*, ISBN 978-3-200-01636-1, pp 45 – 47, Wien (2009)
13. E. Slogsnat, K.-H. Brenner, "Non-stereoscopic method for deflectometric measurement of reflecting surfaces", *DGaO-Proceedings* (Online-Zeitschrift der Deutschen Gesellschaft für angewandte Optik e. V.), ISSN: 1614-8436, 110. Jahrestagung in Brescia/Italien, (2009)
14. D. Wohlfeld, E. Slogsnat, K.-H. Brenner, "Integrated beam splitters for array microscopy in life science", *DGaO-Proceedings* (Online-Zeitschrift der Deutschen Gesellschaft für angewandte Optik e. V.), ISSN: 1614-8436, 110. Jahrestagung in Brescia/Italien, (2009)
15. F. Merchán, D. Wohlfeld, K.-H. Brenner, "High speed communication using micro optical integration", *DGaO-Proceedings* (Online-Zeitschrift der Deutschen Gesellschaft für angewandte Optik e. V.), ISSN: 1614-8436, 110. Jahrestagung in Brescia/Italien, (2009)
16. M. Auer, K.-H. Brenner, "Treatment of spatially varying Permeabilities with the RCWA-Application to Negative-Index Materials", *DGaO-Proceedings* (Online-Zeitschrift der Deutschen Gesellschaft für angewandte Optik e. V.), ISSN: 1614-8436, 110. Jahrestagung in Brescia/Italien, (2009)
17. Xiyuan Liu, Karl-Heinz Brenner, "Guide structures for splicing single-mode fibres fabricated using deep lithography", *Photonik international* 2009/2, pp. 42-43, (2009)

18. F. Merchán, D. Wohlfeld, K.-H. Brenner, "Micro integration of optical systems for the fabrication of active optical cables", 3rd EOS Topical Meeting on Optical Microsystems (OMS09), ISBN 978-3-00-024191-8, (2286), 27.-30.09.09.Capri/Italien (2009).
19. INVITED: Karl-Heinz Brenner, "General Solution Of Two-Dimensional Beam-Shaping With Two Surfaces", 8. International Workshop on Information Optics (WIO'09), 20.-24.06.09 in Paris / France, *Journal of Physics (IOP): Conference Series*, Vol. 206 (012021), doi # 10.1088/1742-6596/206/1/012021, ISSN 1742-6596, <http://iopscience.iop.org/1742-6596/206/1/012021/>, ISSN 1742-6588 (print), (2010)
20. M. Fertig, K.-H. Brenner, "The Vector wave propagation method (VWPM)", *JOSA A*, Vol. 27, No. 4, pp. 709 – 717, (2010)
21. M. Auer, K.-H. Brenner, N. Moll, T. Morf, M. Fertig, T. Stöferle, R.F. Mahrt, J. Weiss, T. Pflüger, „Enhancement of Photo-Detector Responsivity in Standard SOI CMOS Processes by introducing Resonant Grating Structures“, EOS Topical Meeting on Diffractive Optics, 14.-18.02.2010, Koli/Finnland, ISBN 978-3-00-024193-2, (2010)
22. K.-H. Brenner, "General Solution Of Two-Dimensional Beam-Shaping With Two Surfaces", *Information Optics and Photonics*, Springer Verlag, Part 1, pp. 3-11, DOI: 10.1007/978-1-4419-7380-1_1, (2010)
23. F. Merchán, D. Wohlfeld, K.-H. Brenner, "Micro integration of optical components for the fabrication of active optical cables", *Journal of the European Optical Society - Rapid Publications*, Vol. 5, Pub.nr. 10056 (2010)
24. F. Merchán, Karl Heinz Brenner, Peter Gregorius, Sven Hendrik Voß, "FPGA-Board and Active Optical Cable Design for Multi-Gigabit Communication", ESTC 2010 (Electronics System Integration Technology Conferences), Digital Proceedings, poster session 1, p0032 (2010)
25. F. Merchan, X. Liu, K.-H. Brenner, "Effiziente Faserkopplung mit Gradientenindex-Stablinsen", *DGaO-Proceedings* (Online-Zeitschrift der Deutschen Gesellschaft für angewandte Optik e. V.), ISSN: 1614-8436, 111. Jahrestagung in Wetzlar, (2010)
26. E. Slogsnat, R. Buschlinger, K.-H. Brenner, "Miniaturisierte parallele Mikroskopie in der Systembiologie", *DGaO-Proceedings* (Online-Zeitschrift der Deutschen Gesellschaft für angewandte Optik e. V.), ISSN: 1614-8436, 111. Jahrestagung in Wetzlar, (2010)

27. F. Merchán, K.-H. Brenner, R. Börret, U. Berger, „Cost optimized fabrication of Micro-Optical Couplers“, *Optical Fabrication and Testing (OF&T)*, OSA, Technical Digest, ISBN 978-1-55752-893-3, 13.-16-06.2010, Jackson Hole, Wyoming, USA, (2010)
28. Karl-Heinz Brenner, „Aspects for calculating local absorption with the rigorous couple-waved method“, *Optics Express*, Vol. **18**, Iss. 10, pp. 10369-10376, (2010)
29. D. Wohlfeld, K.-H. Brenner, U. Brüning, „Über optische Verbinder und dessen Herstellung“ UHD07a, DE 10 2010 018 248.6, angemeldet
30. R. Buschlinger, K.-H. Brenner, „Light Focusing by binary phase gratings“, 5th EOS Topical Meeting on Advanced Imaging Techniques (AIT), ISBN 978-3-00-030503-0, 29.06.-02.07.2010, Engelberg/Ch (2010)
31. INVITED: Karl-Heinz Brenner, Robert Buschlinger, “Fractal diffraction and focusing properties of binary phase gratings”, 9. Euro-American Workshop on Information Optics (WIO 2010), *IEEE*, ISBN 978-1-4244-8227-6/10, 12.-16. Juli 2010, Helsinki / Finnland, (2010)
32. K.-H. Brenner, „Vorrichtung und Verfahren zur Strahlungskonzentration“, eingereicht beim Europ. Patentamt München, AZ PCT/EP2010/006070, 05.10.2010
33. F. Merchán, K.-H. Brenner, P. Gregorius, S.-H. Voß, „FPGA-Board and Active Optical Cable Design für optische Multi-Gigabit Übertragung“, PLUS 12 / 2010 (*Produktion von Leiterplatten und Systemen / Fachzeitschrift für Aufbau u. Verbindungstechnik in der Elektronik*, Leuze Verlag), Band 12, ISSN 1436-7505 B 49475, pp. 2800-2809, (2010)

Imprint

Publisher:

Prof. Dr. Karl-Heinz Brenner
Chair of Optoelectronics
Institute for Computer Engineering (ZITI)
Ruprecht-Karls-Universität Heidelberg
B6, 23-29, Bauteil C
68131 Mannheim



+49 (0) 621 181 2700



+49 (0) 621 181 2695



<http://oe.ziti.uni-heidelberg.de>

Layout:

Sabine Volk

Kind of publication:

Online

Publication date:

2012